

# Nearby Galaxies and the *Ginga* X-ray Background

F.J. Carrera<sup>1</sup>, X. Barcons<sup>2</sup>, J.A. Butcher<sup>3</sup>, A.C. Fabian<sup>4</sup>, O. Lahav<sup>4</sup>, G.C. Stewart<sup>3</sup>, & R.S. Warwick<sup>3</sup>

<sup>1</sup> *Mullard Space Science Laboratory – University College London, Holmbury St. Mary, Dorking, Surrey, RH5 6NT*

<sup>2</sup> *Instituto Mixto (Consejo Superior de Investigaciones Científicas–Universidad de Cantabria), 39005 Santander, Spain*

<sup>3</sup> *X-ray Astronomy group, Physics Department, University of Leicester, Leicester LE1 7RH*

<sup>4</sup> *Institute of Astronomy, Madingley Road, Cambridge CB3 0HA*

Submitted to *Monthly Notices of the Royal Astronomical Society*

## ABSTRACT

We present here the results of cross-correlating the X-ray background measured by *Ginga* in the 2–10 keV band with several catalogues of extragalactic objects. Positive signals with an amplitude of a few per cent have been found for some catalogues implying that some fraction of the X-ray background is produced either by the class of catalogued sources or by other classes spatially related to them. Detailed X-ray background simulations have been used to assess the significance of the results and, for the first time, the full angular shape of the cross-correlation. The inferred X-ray volume emissivity in the local Universe,  $j_0$ , has been

estimated for two galaxy catalogues (UGC and IRAS) for which the cross-correlation is highly significant. We obtain  $j_0 = (0.74 \pm 0.07)$  for UGC and  $j_0 = (1.15 \pm 0.10)$  for IRAS, in units of  $10^{39} h \text{ erg s}^{-1} \text{ Mpc}^{-3}$ . Extrapolating this result back to  $z \sim 1 - 4$  leads to the conclusion that  $\lesssim 10 - 30$  per cent of the X-ray background could be produced by a non-evolving population of galaxies. These values are shown to be consistent with upper limits on the Auto Correlation Function derived here.

## 1 INTRODUCTION

The puzzle of the origin of the X-ray background (XRB) still remains unsolved, although it is becoming apparent that no single class of ‘miraculous’ sources is able to satisfy simultaneously all the observational constraints accumulated over the last 30 years (see Fabian and Barcons 1992 for a review).

The fraction of the XRB directly resolved into sources in the ‘soft’ band ( $< 2$  keV) is about 50 per cent in the deepest ROSAT surveys (Hasinger *et al.* 1993, Branduardi-Raymont *et al.* 1994). The brightest of these sources (i.e., those with 0.5–2 keV fluxes  $\gtrsim 10^{-14}$  erg cm $^{-2}$  s $^{-1}$ ) are expected to be quasars with  $z \leq 2.5$  (based on the optical identification work of Shanks *et al.* 1991). Optical identification programs are being carried out in order to establish the nature of the sources at and below that flux. On the other hand, fluctuation studies of these Deep *Rosat* fields (Hasinger *et al.* 1993, Barcons *et al.* 1994) reveal the imprint of  $\sim 1000$  sources deg $^{-2}$ , ‘resolving’ a fraction of  $\sim 70$  per cent of the soft XRB. The nature of the sources at fluxes  $\sim 10^{-15}$  erg cm $^{-2}$  s $^{-1}$  will not be known until X-ray telescopes more sensitive than *Rosat* become available.

The lack of imaging devices in the ‘hard’ band (2–10 keV) has made the directly resolved fraction of the XRB in that band much smaller, only a few per cent (Piccinotti *et al.* 1982). Integrating and extrapolating the obtained luminosity functions, clusters of galaxies would contribute  $\sim 4$  per cent of it and AGN (mostly Seyfert galaxies)  $\sim 20$  per cent. Although soon ASCA, and SPECTRUM–X– $\Gamma$  in the future, are expected to give some insight into this problem, useful information is available contained in the angular distribution of the intensity of the XRB (fluctuations and anisotropies).

Fluctuation studies using *Ginga* data (Butcher *et al.* 1994) have shown that the  $\log N - \log S$  curve is consistent with an euclidean shape (sources per unit flux and unit solid angle  $n(S) \propto S^{-2.5}$ ) down to  $\sim 10^{-12}$  erg cm $^{-2}$  s $^{-1}$  (2–10 keV). Recent XRB anisotropies and excess fluctuations studies have shown that only 60–70 per cent of the ‘hard’ band XRB can be produced by sources clustering on scales  $\sim 6 h^{-1}$  Mpc ( $H_0 = 100 h$  km s $^{-1}$  Mpc $^{-1}$ ) (see Danese *et al.* 1992 for a recent review). This implies that the obvious solution of just ‘adding’ more QSOs until the XRB saturates does not trivially work.

A complementary way of facing the problem of the origin of the XRB is to

search for cross-correlations of the XRB intensities with positions of known sources in existing catalogues.

We define the cross-correlation function (CCF) as

$$W_{\text{xg}}(\theta) = \frac{\langle \delta N \cdot \delta I \rangle_{\theta}}{\langle N \rangle \langle I \rangle}, \quad (1)$$

$\delta N$  being the fluctuation in projected galaxy density and  $\delta I$  the XRB deflection,  $\langle N \rangle$  and  $\langle I \rangle$  being the mean projected galaxy density and XRB intensity, respectively (see Sections 2 and 3 for definitions).  $\langle \rangle_{\theta}$  means an average among all those pairs distant an angle  $\theta$ .

Jahoda *et al.* (1991) obtained a value of  $3 \times 10^{-3}$  for the zero-lag cross-correlation function (CCF) of the 2–10 keV XRB intensities (as observed by HEAO–1) with ESO and UGC galaxies. Jahoda *et al.* (1992), using this value, concluded that a substantial fraction of the ‘hard’ XRB could be produced by a non-evolving population of X-ray sources.

Lahav *et al.* (1993) performed a more sophisticated but preliminary analysis of *Ginga* and HEAO–1 data at zero-lag. They arrived at the conclusion that  $\sim 30$ –50 per cent of the ‘hard’ XRB could be produced by local non-evolving X-ray sources. Their analysis (unlike that by Jahoda *et al.* 1992) took into account the clustering of the sources, which, as shown there and in Section 4, can significantly reduce the values of the emissivity deduced from the observed CCFs.

Miyaji *et al.* (1994) obtained  $j_0 = (0.9 \pm 0.2) \times 10^{39} h \text{ erg s}^{-1} \text{ Mpc}^{-3}$  using the zero-lag CCF of the whole sky *HEAO–1* XRB observations with two catalogues of IRAS galaxies. They also used a sample of AGN detected by *HEAO–1* (Grossan 1992) to study the spatial correlation function and the selection function of sources detected both in X-rays and infrared wavelengths.

In the present paper we have analyzed the CCF obtained from a set of *Ginga* scan data (see Section 2.1) with nine catalogues of extragalactic sources (listed in Section 2.2). We have used, for the first time, the full angular shape of the CCF up to 5 degrees to gather information about possible sources of the 2–10 keV XRB and their relation to the sources in the catalogues. We have also taken into account the limits imposed by the observed auto-correlation function (ACF) of the XRB over the same region of the sky.

In Section 3 we show how the CCF of the XRB with the galaxy catalogues is obtained. We also discuss the significance of the signals seen, basing our arguments on detailed simulations of the X-ray sky and the galaxy catalogues in the region under study (Section 3.2).

Section 4 is devoted to the theoretical framework in which the CCF is modelled. We give the expression of the expected CCF as a function of the properties of the sources (selection functions, spatial correlation functions and emissivities) and the collimator profile ('beam').

Our results are used in Section 5 to estimate the volume emissivity of X-ray sources related to a local population of galaxies. The implications of these results are then addressed in Section 6.

Finally, in Section 7 we summarize our results.

## 2 THE DATA

### 2.1 The X-ray data

Our X-ray sample consists of 5 strips over the North Galactic Pole observed in scan mode with the Large Area Counter (LAC) on board of *Ginga*. Every strip was scanned several times by the satellite, accumulating counts in 16 s time intervals, which correspond to  $\sim 0.2$  degrees angular separation. As consecutive scans in the same strip do not exactly overlap, we actually have measurements of the brightness of the X-ray sky with relative separations smaller than that distance. However, as the collimator profile is only well determined in 0.1 deg steps, we have binned the observed counts in 0.2 deg wide bins. This binning also helps in improving the signal-to-noise ratio.

A more thorough description of the data and their reduction process is given in Carrera *et al.* (1993), our data being a subset of those used in that work. We only stress here that the energy band used (*Ginga* LAC Pulse Height Analyzer -PHA- channels 8–20, corresponding roughly to 4–12 keV), and the high galactic latitude of the sample ( $|b| > 30$  deg), lead to a small contamination by diffuse gas from our galaxy. Furthermore, the extension of this region is small and the angle between it and the dipole direction is 86 degrees, making insignificant any dipole correction because of the Compton-Getting effect (*e.g.*, Boldt 1987). Given that our sample is at a supergalactic latitude  $\sim 40$  degrees, the supergalactic plane do not pose any problems of fair sampling on it.

As the region of the sky scanned is also away from known hard X-ray sources (those of Piccinotti *et al.* 1982), we have a sample of extragalactic diffuse XRB deflections or fluctuations  $\delta I \equiv I - \langle I \rangle$ ,  $\langle I \rangle$  being the mean XRB intensity.

## 2.2 The catalogue samples

A total of 7 galaxy samples have been used in this work, together with the Abell catalogue of clusters of galaxies. The sources from each catalogue with Right Ascension ( $\alpha$ )  $\in [210, 270]$  degrees and Declination ( $\delta$ )  $\in [30, 70]$  degrees have been selected and their positions used to define a set of fluctuations in projected galaxy density ( $\delta N$ ) in the following way: at the same positions and with the same collimator orientation as in the real XRB observations, a series of galaxy number density ( $N$ ) ‘observations’ have been performed. Then they are binned in 0.2 deg wide bins (again in the same way as in the X-ray observations) and their mean value ( $\langle N \rangle$ ) subtracted to give the fluctuations  $\delta N$ .

The number of sources used from each catalogue and the value of  $\langle N \rangle$  for each one of them (in sources beam<sup>-1</sup>) are given in Table 1.

Briefly the catalogues are as follows:

- IRAS: the Meurs and Harmon (1989) catalogue that comprises infrared galaxies selected (using purely colour criteria) from the IRAS Point Source Catalogue (PSC) with 60  $\mu\text{m}$  fluxes  $> 0.7$  Jy. This catalogue was also used by Miyaji *et al.* (1994).
- UGC: the Uppsala General Catalogue (Nilson 1973) of optical galaxies, selecting those whose major angular diameters are greater than 1 arcmin.
- IRASQDOT: IRAS QDOT catalogue taking one in six sources out of a galaxy subsample of the PSC (Rowan–Robinson *et al.* 1990). 97 per cent of the 2163 sources in this catalogue (60  $\mu\text{m}$  fluxes  $> 0.6$  Jy and  $|b| > 10^\circ$ ) have been spectroscopically identified.
- CfA: Centre for Astrophysics redshift catalogue of galaxies (Huchra *et al.* 1983), which happens to partly overlap with the region of the sky observed in X-rays.
- Abell: positions of Abell (1958) clusters. The richnesses of the selected clusters are between 0 and 4, most of them having Richness class 0 or 1.
- IRASZ: Strauss *et al.* (1990) sample of IRAS PSC galaxies complete down to 60  $\mu\text{m}$  fluxes  $> 1.936$  Jy, all with  $|b| > 5^\circ$ . Redshifts are available for these

sources. There are two known AGNs in this catalogue within our sample region; including or excluding them does not make any appreciable difference to the results discussed below (neither does it to those of IRASZS or IRASZSVOL below).

- IRASZS: a selection among galaxies in the IRASZ sample, choosing those with  $500 < cz_{\text{LocalGroup}} < 8000 \text{ km s}^{-1}$ . This is done (Yahil *et al.* 1991) to avoid both local galaxies with possible peculiar velocities and very distant ones, for which the selection function (probability of a source being detected; see Section 4) is very small. This catalogue was also used by Miyaji *et al.* (1994).
- IRASZSVOL: this comprises the same sources as in IRASZS, but we weighted them by the inverse of the selection function at their distances. The idea behind this weighting is to 'compensate' for the sources missing in the sample (the farther away, the more likely to be missing, the smaller the selection function and the larger the weight).

### 3 THE OBSERVED CROSS-CORRELATION FUNCTIONS

#### 3.1 Measurement of the Cross Correlation functions

In Section 1 we defined the CCF as

$$W_{\text{xg}}(\theta) = \frac{\langle \delta N \cdot \delta I \rangle_{\theta}}{\langle N \rangle \langle I \rangle}$$

To evaluate  $\langle I \rangle$  we have used the spectrum of the XRB obtained by Marshall *et al.* (1980). It leads to  $\langle I \rangle = 5.7 \times 10^{-8} \text{ erg cm}^{-2} \text{ s}^{-1} \text{ sr}^{-1}$  in the 2–10 keV band, which corresponds to  $\sim 8 \text{ ct s}^{-1} \text{ beam}^{-1}$  in the LAC PHA channels 8 to 20.

The values of  $W_{\text{xg}}(0)$  in 1 deg bins derived from the different samples are noted in Table 1. The UGC–XRB CCF value is larger than the one obtained by Jahoda *et al.* (1991) ( $W_{\text{xg}}(0) \sim (2 - 5) \times 10^{-3}$ ). Our CCF value for the IRAS and IRASZS are also larger than their equivalents in Miyaji *et al.* (1994). This is hardly surprising, since the CCF is heavily dependent on instrument characteristics ( $I$  is measured in counts  $\text{beam}^{-1}$  and  $N$  in galaxies  $\text{beam}^{-1}$ ). For example, the *Ginga* LAC probes deeper in source counts than *HEAO-1* A2 due to its smaller beam size ( $2^{\circ} \times 1^{\circ}$  and  $3^{\circ} \times 1.5^{\circ}$  respectively). The different beam sizes also have a geometrical effect that contributes to make the signal different (see Section 4).

We have plotted  $W_{\text{xg}}(\theta)$  in 1 deg wide bins for the UGC and IRAS samples in Figs. 1a and 1b, respectively (filled dots). The error bars are from the standard deviation in each bin. As we will show in Section 4, CCF signals (such as those seen in Figs. 1a and 1b) are expected due to the finite size of the *Ginga* LAC collimator ( $\sim 1^\circ \times 2^\circ$ ) and/or to the spatial clustering of the X-ray sources with the galaxies in the samples (see also Lahav *et al.* 1993).

### 3.2 Significance of the Cross Correlation Signal

We have simulated both catalogue samples (simply by reshuffling at random the positions of the objects in them) and X-ray fluctuations to assess the significance of our results. By obtaining the CCFs of these random samples, we can test if purely geometrical effects or random positioning could give rise to the observed CCFs.

The simulated X-ray samples have been obtained by uniformly distributing X-ray sources following the  $\log N - \log S$  curve obtained by Butcher *et al.* (1994) (see also Carrera *et al.* 1993 for a complete description of the simulation process).

All these simulated populations (both X-ray and catalogue) have then been folded through the *Ginga* LAC collimator and the corresponding deflections have been obtained as described in Section 2.2.

The values in the column labelled  $W_{\text{xg,sim}}(0)$  of Table 1 are obtained using 100 simulations of every galaxy sample and 100 simulated XRB samples: the quantities quoted are  $2\sigma$  upper limits (they are the higher of the two values that encompass 95 per cent of the simulated  $W_{\text{xg}}(0)$  for each sample). The CCFs from the samples UGC, IRAS and IRASZS are well above those upper limits, showing that they are  $\gg 2\sigma$  significant, and that they do not come from some chance positioning of the sources in the samples or the X-ray data, nor from some geometrical effect due to the collimator or the way the CCFs have been obtained. The signals for the CfA and IRASZ samples are just about at the  $2\sigma$  significance level.

These differences between the CCFs from different samples reflect their different densities, flux limits and clustering properties, and, of course, their different percentages of/clustering with X-ray sources giving rise to the XRB.

In Figs. 1a (UGC) and 1b (IRAS) the medians of the simulated CCFs ( $W_{\text{xg,sim}}(\theta)$ ) are shown as solid lines, as well as values encompassing 68 per cent (dashed lines) and 95 per cent (dotted lines) of the simulations.

To test whether most of the signal is due to a few sources just unresolved in X-rays, we also calculated the CCF (both real and simulated) excluding the five per cent higher X-ray deflections. Both UGC and IRAS CCFs were still above 97 per cent of the simulations, but IRASZS (and CfA and IRASZ) was well below that limit. This, as said earlier, indicates that the CCF signal found for IRASZS was due to a few ‘bright’ X-ray sources just unresolved, while the UGC and IRAS signals come from the sources in those samples as a population. Therefore, we pay special attention to the understanding of these signals.

The simulated CCFs have also been used to estimate the error bars for the observed CCFs at each angular separation (from the 68 per cent limits for each simulation). These are shown in Figs. 2*a* and 2*b* (see Section 5).

Having checked and established the significance of the observed CCFs, their relationship to the properties of the (catalogue and X-ray) sources will be outlined in next section.

## 4 THE THEORETICAL CROSS-CORRELATION FUNCTION

In order to model the CCF on the basis of the relationship between the X-ray sources responsible for the observed fluctuations in the X-ray sky and the catalogued optical/IR sources, let us consider two (distinct) source populations. The first one would consist of galaxies with selection function  $P(r)$  (probability of a source being detected at a distance  $r$  from the observer) and mean spatial density  $\langle n_g \rangle$ . Our second population would consist of X-ray sources with local volume emissivity  $j_0$  (emitted X-ray power per unit volume) and clustered with the above galaxies, with a spatial cross-correlation function  $\xi_{\text{xg}}(\mathbf{r}_g - \mathbf{r}_x)$  (probability in excess of a purely poissonian distribution that a galaxy and an X-ray source lie at a distance  $|\mathbf{r}_g - \mathbf{r}_x|$ ). We will assume, as usual, a form  $\xi_{\text{xg}}(r) = (r/r_0)^{-\gamma}$  for  $\xi_{\text{xg}}(r)$ .  $\xi_{\text{xg}}(r) = 0$  (or equivalently,  $r_0 = 0$ ) would mean that these two populations are independently distributed in the sky.

Some of the X-ray sources may be actually present in the catalogue. In this case X-ray and catalogue observations in different directions (given by the unit vectors  $\mathbf{n}_x$  and  $\mathbf{n}_g$  respectively) would be correlated when viewed through a collimator with profile  $G(\mathbf{n}_x - \mathbf{n}_g)$ . If we define

$$\eta(\mathbf{n}_x - \mathbf{n}_g) = \langle I \rangle \cdot \langle N \rangle \cdot W_{\text{xg}}(\mathbf{n}_x - \mathbf{n}_g) \quad (2)$$

then the correlation term without taking into account the possible clustering of the catalogued sources (poissonian term) would be

$$\eta_{\text{pois}}(\mathbf{n}_x - \mathbf{n}_g) = \int dr r^2 \frac{j_{\text{xg}}}{4\pi r^2} P_x(r) \int d^2\Omega_n G(\mathbf{n} - \mathbf{n}_x) G(\mathbf{n} - \mathbf{n}_g) \quad (3)$$

where  $j_{\text{xg}}$  ( $\leq j_0$ ) is the local X-ray volume emissivity of the galaxies that are also X-ray emitters (we have assumed that  $j_{\text{xg}}$  is constant within the galaxy sample depth) and  $P_x(r)$  their selection function. Defining the effective catalogue depth as

$$R_* = \int dr P_x(r) \quad (4)$$

and the collimator autocorrelation function (ACF) as

$$\eta_{\text{col}}(\mathbf{n}_x - \mathbf{n}_g) = \int d^2\Omega_n G(\mathbf{n} - \mathbf{n}_x) G(\mathbf{n} - \mathbf{n}_g) \quad (5)$$

then

$$\eta_{\text{pois}}(\mathbf{n}_x - \mathbf{n}_g) = \frac{1}{4\pi} j_{xg} R_* \eta_{\text{col}}(\mathbf{n}_x - \mathbf{n}_g) \quad (6)$$

If we now allow for clustering among the two populations, the CCF is

$$\eta_{\text{clus}}(\mathbf{n}_x - \mathbf{n}_g) = \int dV_{x'} \frac{j_0}{4\pi r_{x'}^2} \int dV_{g'} P(r_{g'}) \langle n_{g'} \rangle G(\mathbf{n}_{x'} - \mathbf{n}_x) G(\mathbf{n}_{g'} - \mathbf{n}_g) \xi(\mathbf{r}_{x'} - \mathbf{r}_{g'}) \quad (7)$$

which, under the small angle approximation and using Eq. 5, leads to

$$\eta_{\text{clus}}(\mathbf{n}_x - \mathbf{n}_g) = \frac{1}{4\pi} j_0 \langle n_g \rangle H_\gamma r_0^\gamma \int dr r^{3-\gamma} P(r) \int d^2\Omega_n \eta_{\text{col}}(\mathbf{n} - \mathbf{n}_x) |\mathbf{n} - \mathbf{n}_g|^{1-\gamma} \quad (8)$$

where again we have assumed a constant  $j_0$  over the volume of the galaxy sample and  $H_\gamma = \Gamma(1/2)\Gamma((\gamma - 1)/2)/\Gamma(\gamma/2)$ ,  $\Gamma$  being the gamma function.

The total CCF would then be the sum of these two terms (Eqs. 6 and 8). If clustering is present, but its contribution neglected, the volume emissivity is grossly overestimated (by as much as a factor of 6 in the relevant case). Eq. 8 generalizes Eqs. 2 and 3 in Lahav *et al.* (1993) paper for the non-zero lag non-square collimator case. Note that the emissivity ( $j_0$  in this paper) was denoted as  $\rho_x$  in that paper.

For the UGC and IRAS samples the selections functions are well determined (Hudson and Lynden-Bell 1991 and Yahil *et al.* 1991 respectively).

Miyaaji *et al.* (1994) constructed the spatial correlation function of a sample of *HEAO-1* X-ray sources with the IRAS catalogue, obtaining  $\gamma = 1.8$  and  $r_0 = 4 h^{-1}$  Mpc. They also derived the selection function for the X-ray sources that were also in the IRAS 0.7 Jy sample (of which our IRAS sample is a subset)  $P_x(r)$ , obtaining a value of  $R_* = 65 h^{-1}$  Mpc. These are the values of  $\gamma$ ,  $r_0$  and  $R_*$  that we have used for our IRAS sample.

For the UGC sample we have assumed  $P_x(r) = P(r)$  (the selection function of the X-ray emitting galaxies in the UGC catalogue is the same as the global one) for simplicity, since its real value is not known. Furthermore, we have used the spatial correlation function of the optical galaxies as the cross-correlation function of them with the X-ray sources, *i.e.*,  $\gamma = 1.8$  and  $r_0 = 5 h^{-1}$  Mpc.

Finally, in order to minimize the number of free parameters, we have assumed  $j_{\text{xg}} = j_0$  (the X–ray sources are all galaxies, and they are clustered like the galaxies of the catalogue). The effects of this assumption are discussed in Section 6.

Taking into account all the above assumptions, from Eqs. 6 and 8 we obtain

$$\eta(\mathbf{n}_x - \mathbf{n}_g) = \frac{j_0}{4\pi} \left( R_* \eta_{\text{col}}(\mathbf{n}_x - \mathbf{n}_g) + \langle n_g \rangle H_\gamma r_0^\gamma \int d^3r r^{3-\gamma} P(r) \int d^2\Omega_n \eta_{\text{col}}(\mathbf{n} - \mathbf{n}_x) |\mathbf{n} - \mathbf{n}_g|^{1-\gamma} \right) \quad (9)$$

The value of  $\langle n_g \rangle$  is easily calculated taking into account

$$\langle N \rangle = \int d^3r P(r) G(\mathbf{n}) \langle n_g \rangle = \Omega_{\text{eff}} \cdot \int dr r^2 P(r) \cdot \langle n_g \rangle \quad (10)$$

where  $\Omega_{\text{eff}} = \int d^2\Omega_n G(\mathbf{n})$  is the effective solid angle of the collimator (in our case  $5.7 \times 10^{-4}$  sr), and the values of  $\langle N \rangle$  are listed in Table 1.

The collimator profile of the *Ginga* LAC is well known down to scales  $\sim 0.1$  degrees, but unfortunately the geometry of the X–ray observations is quite complex, involving many different relative positions and orientations of the collimator. We have then obtained  $\eta_{\text{col}}(\theta)$  from the set of simulations of X–ray sources previously used to estimate the significance of the observed CCFs, and using the relation  $\langle \delta I \cdot \delta I \rangle_\theta = \langle S^2 \rangle \cdot \eta_{\text{col}}(\theta)$  where  $\langle S^2 \rangle$  is the mean of the square of the X–ray flux  $S$  as calculated from the  $\log N - \log S$  curve used in the simulations (see Section 3.2). In this way we obtain a collimator ACF ‘tailored’ to our needs, including all the geometrical effects of our X–ray data.

Finally, the ‘zero’ level of the CCF (*i.e.*, the cross–correlation expected in the absence of any true cosmic signal) is not zero because the finite size of the sample introduces a negative baseline in the correlation functions (Kondo 1990). This zero level ( $= -W_{\text{xg}}(0) / \langle \text{Number of pairs at zero-lag} \rangle$ ) has been calculated and subtracted from the observed CCF before fitting.

## 5 RESULTS: THE VOLUME EMISSIVITY

Although our angular bin size (0.2 deg) provides us with many bins, they are hardly independent (due to the collimator extension and to the fact that we are dealing with the product of pairs of observations each of which appear in many pairs). Therefore, we have only kept one free parameter ( $j_0$ ). Its value has been obtained by fitting (using minimum least squares) the model given in Eq. 9 to the observed CCF binned in 0.2 degree bins. This has been done for two different angular ranges (0.2  $\rightarrow$  2 deg and 0.2  $\rightarrow$  5 deg) and for several values of  $R_{\min}$ , which corresponds to the distance beyond which the selection function drops below one ( $P(r < R_{\min}) = 1$ ), *i.e.*, galaxies begin to be lost or undetected. The results are shown in Table 2.

There is a significant difference between fits to the different angular ranges: this is because  $\eta_{\text{clus}}(\theta)$  is significantly different from zero between 2 and 5 degrees and then the fitting over the larger range is bound to require a lower normalization ( $\rightarrow$  lower  $j_0$ ). This is shown in Figs. 2a (UGC) and 2b (IRAS) where the models marked with an asterisk in Table 2 are plotted along with the observed CCFs: the solid lines correspond to the total CCFs, while dashed lines are the clustering terms and dotted lines the poissonian ones. The error bars on the observed CCFs are from the simulations of Section 3.2.

The peaks visible in Figs. 2a and 2b at about 1.6 degrees in the observed CCFs are very probably due to an X-ray source just unresolved that happens to fall between two of our strips. If the simulations explained above are repeated with 0.2 deg bins, that peak is also seen in 5 out of a 100 simulations. A similar effect (due to the overlapping of the long sides of the collimator in every two adjacent strips) is seen in the poisson CCFs.

From the results in Table 2, the UGC sample yields an X-ray volume emissivity  $j_0 = (0.74 \pm 0.08 \pm 0.13) \times 10^{39} h \text{ erg s}^{-1} \text{ Mpc}^{-3}$  while the IRAS one gives  $j_0 = (1.15 \pm 0.10 \pm 0.19) \times 10^{39} h \text{ erg s}^{-1} \text{ Mpc}^{-3}$ . These values are in good agreement with the zero-lag results obtained by Lahav *et al.* (1993). The errors given are the 1 and 2 $\sigma$  confidence levels obtained with bootstrap simulations: for each angular bin in  $W_{\text{xg}}$  we have extracted at random (and replaced) as many pairs  $(\delta I, \delta N)$  as in the real data and calculated  $\langle \delta N \cdot \delta I \rangle_\theta / \langle N \rangle \langle I \rangle$ . This was repeated 1000 times and the resulting CCF was fitted to Eq. 9 to obtain  $j_0$ ; the quoted errors enclose 68.3 per cent (1 sigma)

and 95.4 per cent (2 sigma) of the simulations. They also span the range of values of  $j_0$  in Table 2 obtained for each sample, reflecting thus not only the statistical errors in our fits, but also uncertainties in our model parameters ( $R_{\min}, \gamma, r_0$ ).

If we had ignored the clustering term (as did Jahoda *et al.* 1991), we would have obtained  $j_0 \sim 8 \times 10^{39} h \text{ erg s}^{-1} \text{ Mpc}^{-3}$  for UGC, showing the importance of taking it into account.

The value found by Miyaji *et al.* (1994) ( $j_0 = (0.9 \pm 0.2) \times 10^{39} h \text{ erg s}^{-1} \text{ Mpc}^{-3}$ ) is in good agreement with our IRAS result (they overlap within 1 sigma), taking into account the different IRAS sample (our 0.7 Jy versus their 2 Jy with a local cutoff), the different instrument (*Ginga* LAC versus *HEAO-1* A2), the slightly different observation bands (4–12 keV versus 2–10 keV) and the different techniques (full angular and collimator resolution versus zero-lag square collimator) used.

## 6 IMPLICATIONS FOR THE X-RAY BACKGROUND

In this section we study the fraction of the XRB contributed by the sources whose emissivity we have just obtained from their CCF with optical and IR galaxies.

The intensity received from objects with local volume emissivity  $j_0$  distributed up to redshift  $z_{\max}$  is

$$I(< z_{\max}) = \frac{\Omega_{eff}}{4\pi} \frac{c}{H_0} j_0 f(z_{\max}, \Omega_0, p, \alpha) \quad (11)$$

where  $f$  is the effective look-back factor (Boldt 1982, Lahav 1992) which depends on the cosmology ( $\Omega_0=1$ ), on the X-ray spectrum of the sources (we assume a power law with energy index  $\alpha = 0.7$  which is consistent with the XRB fluctuations studied by Butcher *et al.* 1994), on the evolution of the emissivity (comoving  $j(z) = j_0(1+z)^p$ ) and, of course, on the maximum redshift of integration  $z_{\max}$ . Under this assumptions, we get

$$I(< z_{\max}) = \frac{\Omega_{eff}}{4\pi} \frac{c}{H_0} j_0 \int_0^{z_{\max}} dz (1 + \Omega_0 z)^{-1/2} (1 + z)^{-2-\alpha+p} \quad (12)$$

The fraction of the XRB contributed by those objects is then  $F \equiv I(< z_{\max})/\langle I \rangle$ . In Figs. 3a and 3b we show contour plots for different values of  $F$  (for  $j_0 = 0.74$  and  $1.15 \times 10^{39} h \text{ erg s}^{-1} \text{ Mpc}^{-3}$ , UGC and IRAS best fits respectively) in the  $(z_{\max}, p)$  space. We can see that between 10–20 per cent of the XRB could be produced if we extrapolate the obtained emissivity to  $z_{\max} = 1$ , and 20–30 per cent

if  $z_{\max} = 4$ , in the absence of evolution ( $p = 0$ ). Some moderate positive evolution would lead to much higher values (but see below). Note that Eq. 12 only depends on  $-\alpha + p$ , not on their individual values, so if a different spectral slope  $\alpha'$  is considered, the corresponding  $F$  would be given at ( $z_{\max}, p' = p - \alpha' + 0.7$ ).

The population of sources whose emissivity has been obtained would also produce some auto-correlation signal on their X-ray intensities (ACF). Any estimation of their contribution to the XRB must be consistent with the current upper limits on the ACF. We have derived (Fig. 4) the non poissonian ACF of the X-ray sample in the same way as Carrera *et al.* (1993) (i.e., by subtracting from the observed ACF that expected from a purely poissonian distribution of sources, obtained by simulations). Again, only upper limits to the cosmic signal are obtained, a null value being the best estimate of the non poissonian ACF.

If we assume an evolution for the spatial correlation function of  $\xi(r, z) = (1 + z)^{-3-\epsilon}(r/r_0)^{-\gamma}$ , then under the small angle approximation, the non poissonian ACF is given by

$$W_{xx}(\mathbf{n}_1 - \mathbf{n}_2) = \frac{c}{H_0} \left( \frac{j_0}{4\pi\langle I \rangle} \right)^2 r_0^\gamma H_\gamma \int d^2\Omega_n \eta_{\text{col}}(\mathbf{n} - \mathbf{n}_1) |\mathbf{n} - \mathbf{n}_2|^{1-\gamma} \int_0^{z_{\max}} dz (1 + \Omega_0 z)^{-1/2} (1 + z)^{-5-\epsilon-2\alpha+2p} d_A^{1-\gamma}(z). \quad (13)$$

Or, taking into account Eq. 11

$$W_{xx}(\mathbf{n}_1 - \mathbf{n}_2) = \frac{H_0}{c} \frac{F^2}{\Omega_{eff}^2 f^2(z_{\max}, \Omega_0, p, \alpha)} r_0^\gamma H_\gamma \int d^2\Omega_n \eta_{\text{col}}(\mathbf{n} - \mathbf{n}_1) |\mathbf{n} - \mathbf{n}_2|^{1-\gamma} \int_0^{z_{\max}} dz (1 + \Omega_0 z)^{-1/2} (1 + z)^{-5-\epsilon-2\alpha+2p} d_A^{1-\gamma}(z), \quad (14)$$

where  $d_A(z)$  is the angular distance. In this expression, for a given pair  $(z_{\max}, p)$ , the only free parameter is  $F$ , the fraction of the XRB produced by the objects whose ACF we are studying.

To get a quantitative idea of the constraints that this ACF places on the possible values of  $p$  and  $z_{\max}$ , we have  $\chi^2$ -fitted the observed non-poissonian ACF (Fig. 4) to Eq. 14 over the range 0.2 – 5 deg, with  $F$  as the only free parameter. The best fit (under the current assumptions on the clustering properties of the sources) always

corresponds to  $F = 0$ ; for each pair  $(z_{\max}, p)$  the maximum allowed value of  $F$  (from  $\Delta\chi^2 = 4$  or  $2\sigma$ ) is plotted in Figs. 5a and 5b for comoving and stable clustering ( $\epsilon = -1.2$  and  $\epsilon = 0$ , respectively) and for UGC ( $\gamma = 1.8$  and  $r_0 = 5 h^{-1}$  Mpc). Figs. 5c and 5d correspond (respectively) to the same evolutions of the clustering for IRAS ( $\gamma = 1.8$  and  $r_0 = 4 h^{-1}$  Mpc). Combining Figs. 3 and 5 we can see that the ACF upper limits do not allow contributions to the XRB greater than  $\sim 40 - 50$  per cent, even with evolution.

In Section 4 we assumed that  $j_{\text{xg}} = j_0$ . If we keep both quantities separate,  $j_0$  (the total emissivity) is replaced by  $j_{\text{xg}}$  (the emissivity of the sources in the catalogue) as the free quantity to fit, and  $r_0$  by  $r_0' = r_0(j_0/j_{\text{xg}})^{1/\gamma} > r_0$ . Hence, the net effect of only a fraction of the galaxies being X-ray emitters would be to enhance the importance of the clustering term with respect to the poisson term (as expected). As the clustering term is already dominant for the UGC sample, reducing  $j_{\text{xg}}/j_0$  even down to 25 per cent does not have any effect on the derived total  $j_0$ . However, the poisson term is dominant for the IRAS sample and as we decrease  $j_{\text{xg}}/j_0$  the clustering term takes over. This, in turn, increases the total emissivity (by  $\sim 50$  per cent when  $j_{\text{xg}}/j_0 = 0.25$ ), but the ACF constraints keep  $F \lesssim 20$  per cent.

The difference between the X-ray emissivities obtained for the UGC and IRAS samples is likely to reflect an intrinsic difference in properties of their constituent galaxies. For example, the UGC catalogue selects galaxies by their diameter, without distinction of type, while the IRAS catalogue is a far-infrared selected sample, with a high proportion of star forming and dust rich galaxies, hence mostly spirals.

We know that sources producing the *Ginga* fluctuations have a spectrum with energy index  $\sim 0.7$  (Butcher *et al.* 1994), and these are precisely the sources whose emissivity has been obtained here. With only a moderate contribution to the XRB, the residual spectrum of the XRB would be much flatter than the presently observed one (energy index  $\sim 0.4$ ). This will have wide implications for the sources of this residual XRB, which will need to be highly absorbed and/or reflection dominated.

## 7 CONCLUSIONS

X-ray observations of the 2–10 keV XRB in scan mode performed with the *Ginga* satellite have been cross-correlated with several catalogues of different objects (mainly galaxies). The significance level of the resulting CCF signals have been established using simulations of both X-ray and catalogue samples.

We have concluded that there is a strong cross-correlation between the hard XRB and nearby galaxies (especially those in UGC and the IRAS catalogue or Meurs & Harmon 1989), finding  $W_{\text{xg}}(0) \sim 1.2 - 1.4 \times 10^{-2}$ .

Expressions have been derived for the expected CCF at non-zero lag when the population of X-ray sources dominating the *Ginga* fluctuations are associated or strongly clustered with the catalogued galaxies. In the specific case of the X-ray sources being present in the galaxy catalogue, least-squares fitting has been used to obtain the X-ray volume emissivity  $j_0$  necessary to produce the observed signal, obtaining  $j_0 \sim 0.7 - 1.2 \times 10^{39} h \text{ erg s}^{-1} \text{ Mpc}^{-3}$ .

Extrapolating this emissivity back to  $z = 1$  in the absence of evolution, 10–20 per cent of the XRB would be produced ( $\lesssim 30$  per cent if the contribution from the non-evolving sources is integrated up to  $z = 4$ ). We have shown that these fractions are consistent with the absence of any ACF signal in the XRB.

Higher fractions, close to saturation, would be achieved even with very moderate evolution. However, these high fractions are not permitted by the upper limits on the ACF. Furthermore, the spectrum of the summed contribution of these sources would be very different from the observed XRB spectrum, unless rapid spectral evolution also takes place.

Direct observations with higher angular resolution instruments (*ASCA*, *SPECTRUM-X-Gamma*, *XMM*) would be very useful to decide on whether the emissivities obtained here are actually from the sources in the catalogues, or come from X-ray sources clustered with them. They would also provide spectra for fainter sources, helping to decipher the riddle of the hard X-ray background.

## ACKNOWLEDGEMENTS

XB thanks the DGICYT for financial support, under project PB92-00501. FJC, XB and ACF acknowledge partial financial support from a NATO collaborative research grant. XB and ACF were partly supported by the “Human Capital and Mobility” programme of the EU under contract CHRX-CT92-0033.

## REFERENCES

- Abell, G.O., 1958. *ApJS*, 3, 211
- Barcons, X., Branduardi-Raymont, G., Warwick, R.S., Fabian, A.C., Mason, K.O., Mc Hardy, I., Rowan-Robinson, M., 1994. *MNRAS*, 268, 833
- Boldt, E., 1987. *Phys. Reports*, 146, 215
- Branduardi-Raymont, G., Mason, K.O., Warwick, R.S., Carrera, F.J., Mittaz, J.P.D., Puchnarewicz, E.M., Smith, P.J., Barber, C.R., Pounds, K.A., Stewart, G.C., McHardy, I.M., Jones, L.R., Merrifield, M.R., Fabian, A.C., McMahon, R., Ward, M.J., George, I.M., Jones, M.H., Lawrence, A., Rowan-Robinson, M., 1994. *MNRAS*, 270, 947
- Butcher J.A., *et al.* , 1994. Submitted to *MNRAS*
- Carrera, F.J., Barcons, X., Butcher, J.A., Fabian, A.C., Stewart, G.C., Toffolatti, L., Warwick, R.S., Hayashida, K., Inoue, H., Kondo, H., 1993. *MNRAS*, 260, 376
- Danese, L., De Zotti, G., Andreani, P., 1992. In: *The X-Ray Background*, ed. Barcons, X., Fabian, A.C., Cambridge Univ. Press, p. 61
- Fabian, A.C., Barcons, X., 1992. *ARA&A*, 30, 429
- Hasinger, G., Burg, R., Giacconi, R., Hartner, G., Schmidt, M., Trümper, J., Zamorani, G., 1993. *A&A*, 271, 1
- Grossan, A.G., 1992. PhD Thesis, Massachusetts Institute of Technology
- Huchra, J.P., Davis, M., Latham, D., Tonry, J., 1983. *ApJS*, 52,89
- Hudson, M.J., Lynden-Bell, D., 1991. *MNRAS*, 252, 219
- Jahoda, K., Lahav, O., Mushotzky, R.F., Boldt, E.A., 1991. *ApJ*, 378, L37. Erratum in 1992. *ApJ*, 399, L107
- Kondo, H., 1990. PhD Thesis, University of Tokyo
- Lahav, O., 1992. In: *The X-Ray Background*, ed. Barcons, X. & Fabian, A.C., Cambridge Univ. Press, p. 102

Lahav, O., Fabian, A.C., Barcons, X., Boldt, E., Butcher, J., Carrera, F.J., Jahoda, K., Miyaji, T., Stewart, G.C., Warwick, R.S., 1993. *Nat*, 364, 693

Marshall, F.E., Boldt, E.A., Holt, S.S., Miller, B.B., Mushotzky, R.F., Rose, L.A., Rothschild, R.E., Serlemitsos, P.J., 1980. *ApJ*, 235, 4

Meurs, E.J.A., Harmon, R.T., 1989. *A&A*, 206, 53

Miyaji, T., Lahav, O., Jahoda, K., Boldt, E., 1994. *ApJ*, 434, 424

Nilson, P., 1973. *Uppsala General Catalogue of Galaxies*, Uppsala Astr. Obs. ann., 6

Piccinotti, G. Mushotzky, R.F., Boldt, E.A., Holt, S.S., Marshall, F.E., Serlemitsos, P.J., Shafer, R.A., 1982. *ApJ*, 253, 485

Rowan–Robinson, M., Lawrence, A., Saunders, W., Crawford, J., Ellis, R., French, C.S., Parry, I., Xiaoyang, X., Allington–Smith, J., Efstathiou, G., Kaiser, N., 1990. *MNRAS*, 247, 1

Shanks, T., Georgantopoulos, I., Stewart, G.C., Pounds, K.A., Boyle, B.J., Griffiths, R.E., 1991. *Nat*, 353, 315

Strauss, M.A., Davis, M., Yahil, A., Huchra, J.P., 1990. *ApJ*, 361, 49

Yahil, A., Strauss, M.A., Davis, M., Huchra, J.P., 1991. *ApJ*, 372, 380

## FIGURE CAPTIONS

**Figure 1.**  $W_{\text{xg}}(\theta)$  in 1 degree bins (filled dots): the error bars are extracted from the standard deviation in each bin. Also shown are the median of the simulations (solid line) and the limits encompassing 68 (dashed lines) and 95 (dotted lines) per cent of the simulations.  $a$  is for the UGC sample and  $b$  for the IRAS sample (see text).

**Figure 2.**  $W_{\text{xg}}(\theta)$  in 0.2 degree bins (filled dots): the error bars are extracted from the simulations. Also shown are the best total fit (solid line) and the clustering (dashed line) and poissonian terms (dotted line).  $a$  is for the UGC sample and  $b$  for the IRAS sample. The peaks at about 1.6 degrees present in both observed CCFs are due to a just unresolved X-ray source between observed sky strips (see text).

**Figure 3.** Contour plots (in the  $(z_{\text{max}}, p)$  space) of the fraction of the X-ray background  $F$  produced by a population with local emissivity  $j_0$ : levels of  $F=0.1$  (solid line), 0.3 (dashed line), 0.5 (dot-dashed line), 0.7 (dotted line) and 0.9 (dash-dot-dot line) are shown.  $a$  is for  $j_0 = 0.74$  (UGC) and  $b$  for  $j_0 = 1.15$  (IRAS), both in units of  $10^{39} h \text{ erg s}^{-1} \text{ Mpc}^{-3}$ .

**Figure 4.** Non-poissonian ACF of the XRB: the error bars ( $1\sigma$ ) are extracted from simulations (see text).

**Figure 5.** Contour plots of the maximum  $F$  allowed by the ACF. Levels of  $F=0.1$  (solid line), 0.3 (dashed line), 0.5 (dot-dashed line), 0.7 (dotted line) and 0.9 (dash-dot-dot-dot line) are shown.  $a$  is for comoving clustering and UGC,  $b$  for stable clustering and UGC,  $c$  is for comoving clustering and IRAS and  $d$  for stable clustering and IRAS.

**Table 1.** Cross-correlation functions of several samples with the XRB (see text).

Name	N	$\langle N \rangle$	$W_{\text{Xg}}(0)$	$W_{\text{Xg,sim}}(0)$
UGC	951	1.24	0.0116±0.0015	<0.008
IRAS	351	0.48	0.0142±0.0016	<0.010
IRASQ0	534	0.74	0.0063±0.0013	<0.009
CfA	196	0.32	0.0190±0.0030	<0.018
Abell	210	0.26	0.0100±0.0020	<0.017
IRASZ	82	0.10	0.0240±0.0050	<0.026
IRASZS	45	0.06	0.0460±0.0080	<0.026
IRASZSVOL	45	1.97	0.0060±0.0060	<0.069

**Table 2.** Results of the fitting for different parameters (see text).

Sample	$r_0$ ( $h^{-1}$ Mpc)	$\gamma$	Range fitted (degrees)	$R_{\text{min}}$ ( $h^{-1}$ Mpc)	$j_0 (\pm 1\sigma \pm 2\sigma)$ ( $10^{39} h \text{ erg s}^{-1} \text{ Mpc}^{-3}$ )
UGC	5.00	1.80	0.2,2.0	11.1	0.82
UGC	5.00	1.80	0.2,5.0	11.1	0.65
UGC	5.00	1.80	0.2,2.0	13.3	0.92
UGC*	5.00	1.80	0.2,5.0	13.3	0.74 ( $\pm 0.07 \pm 0.13$ )
IRAS	4.00	1.80	0.2,2.0	1.0	1.22
IRAS	4.00	1.80	0.2,2.0	5.0	1.23
IRAS	4.00	1.80	0.2,2.0	10.0	1.24
IRAS	4.00	1.80	0.2,5.0	1.0	1.14
IRAS*	4.00	1.80	0.2,5.0	5.0	1.15 ( $\pm 0.10 \pm 0.20$ )
IRAS	4.00	1.80	0.2,5.0	10.0	1.17
IRAS	4.00	1.65	0.2,2.0	5.0	1.34
IRAS	4.00	1.65	0.2,5.0	5.0	1.23
IRAS	3.75	1.65	0.2,2.0	5.0	1.40
IRAS	3.75	1.65	0.2,5.0	5.0	1.30

Figure 1a

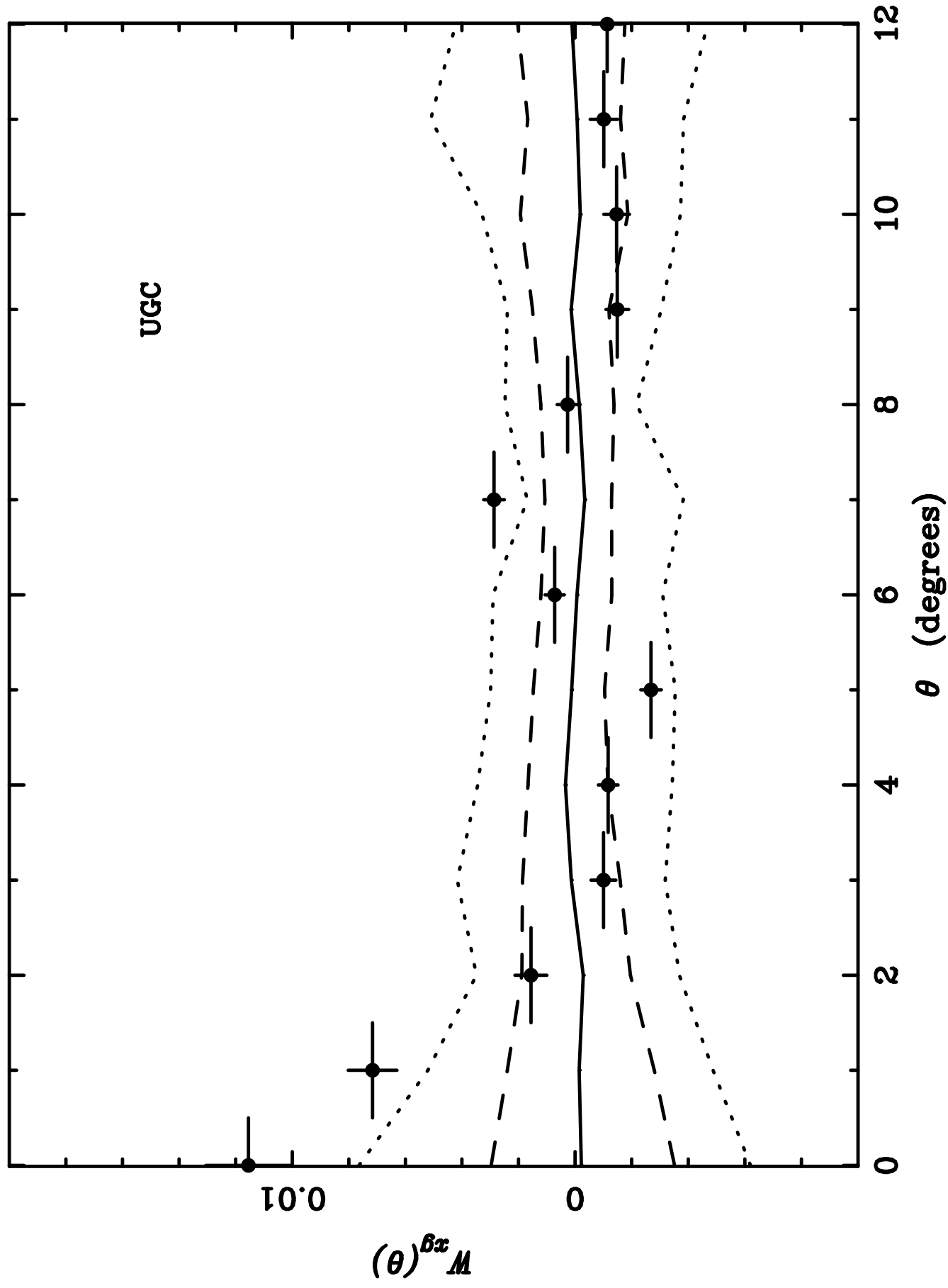


Figure 1b

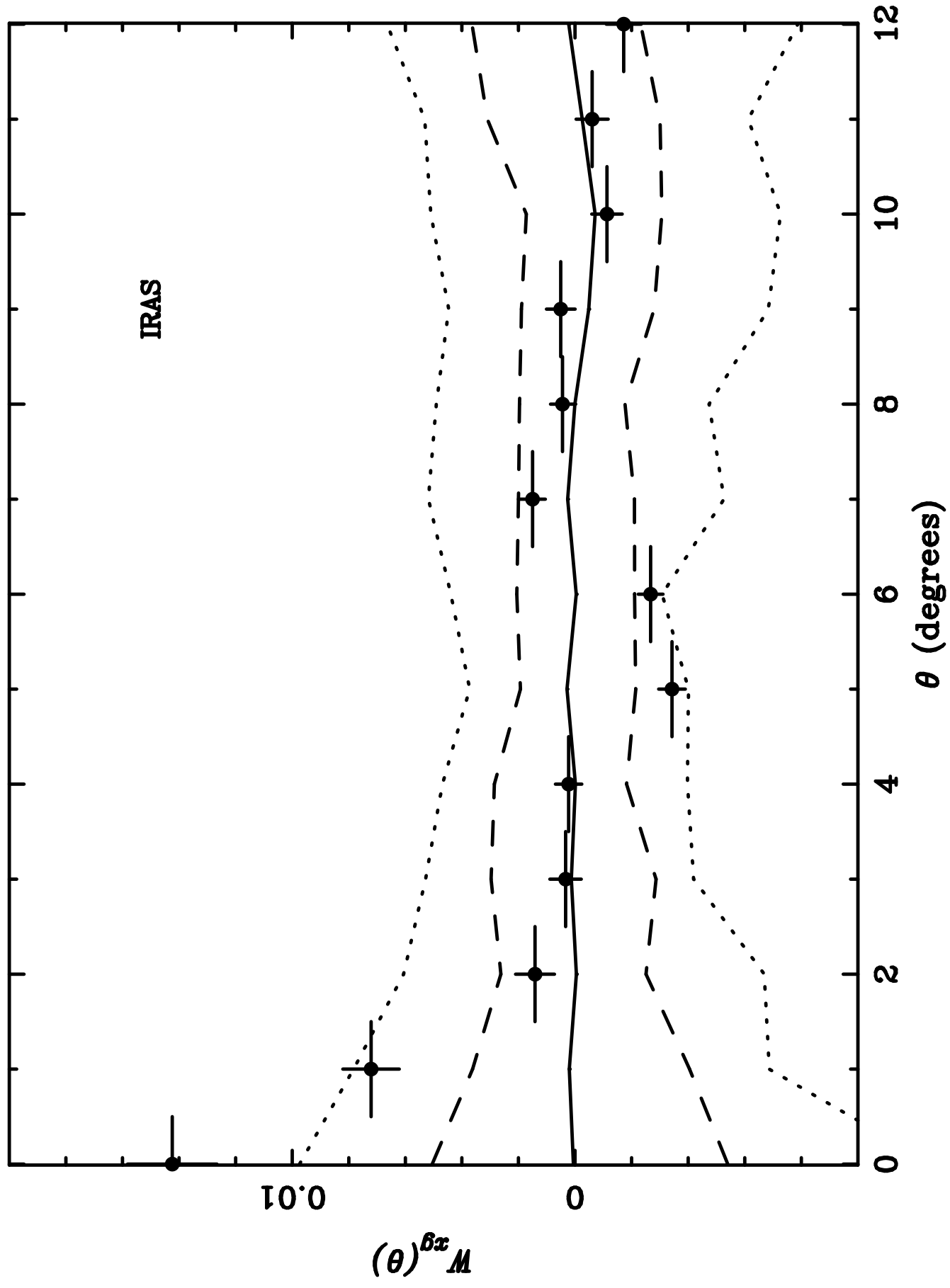


Figure 2a

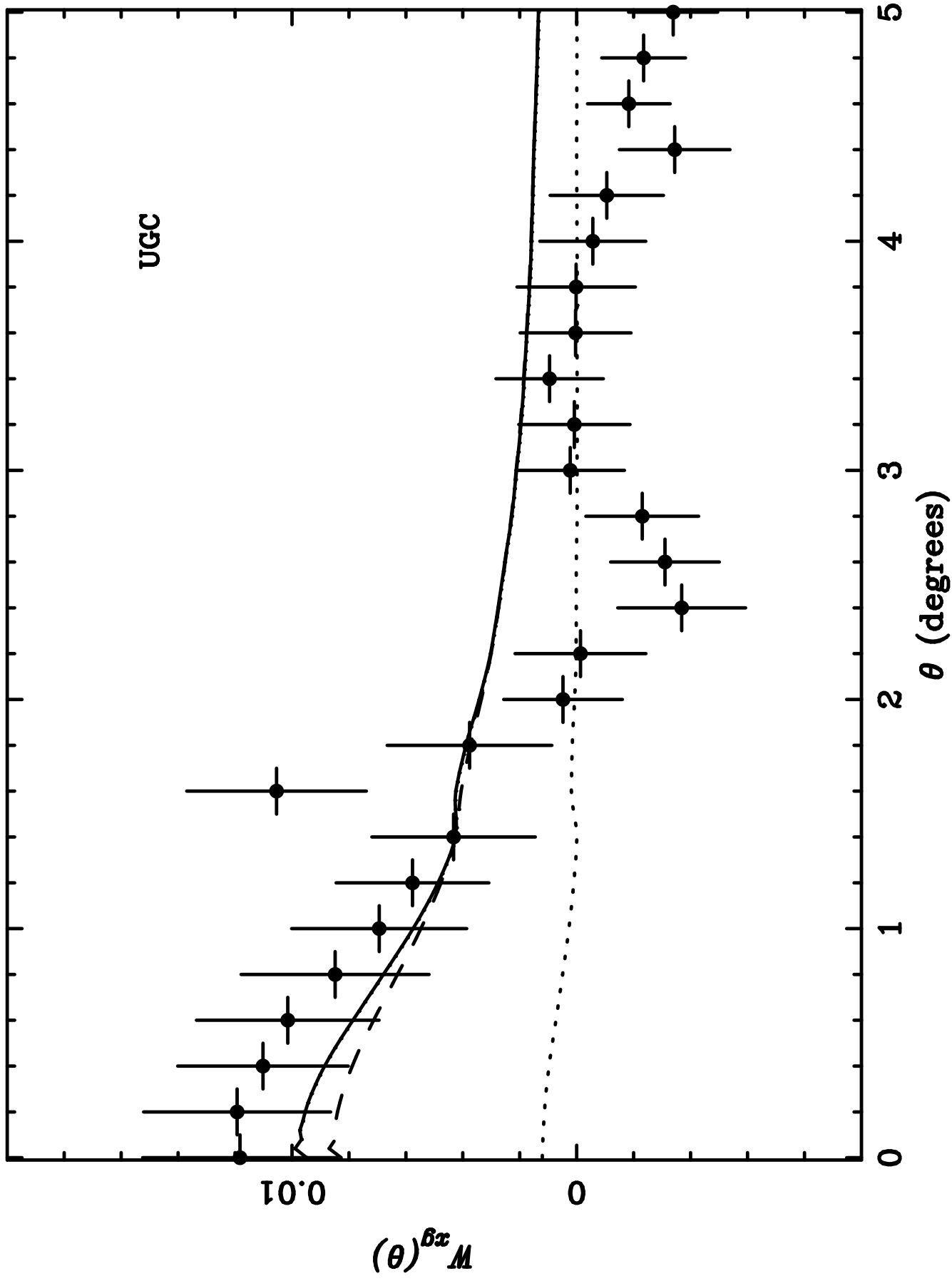


Figure 2b

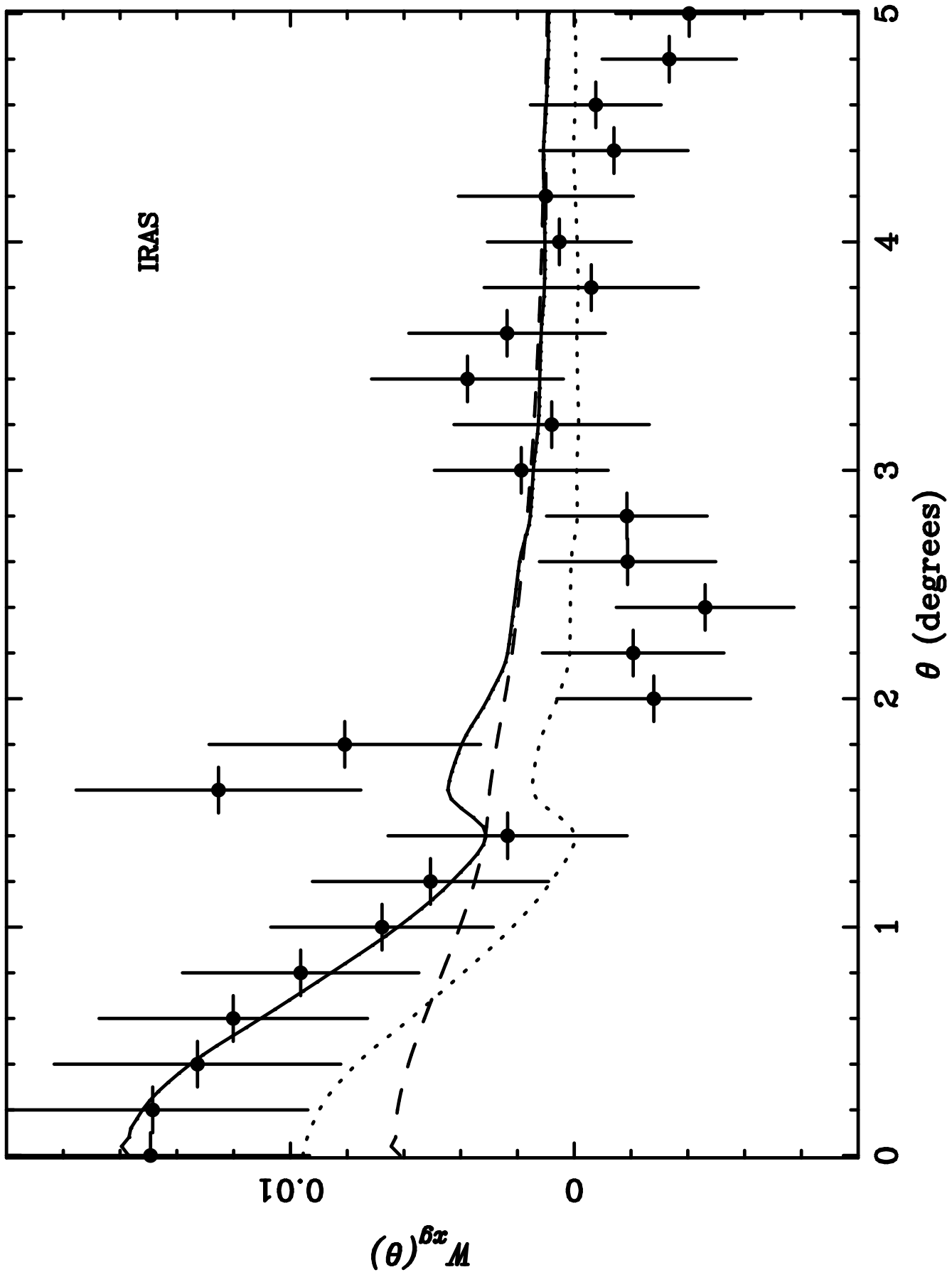


Figure 3a

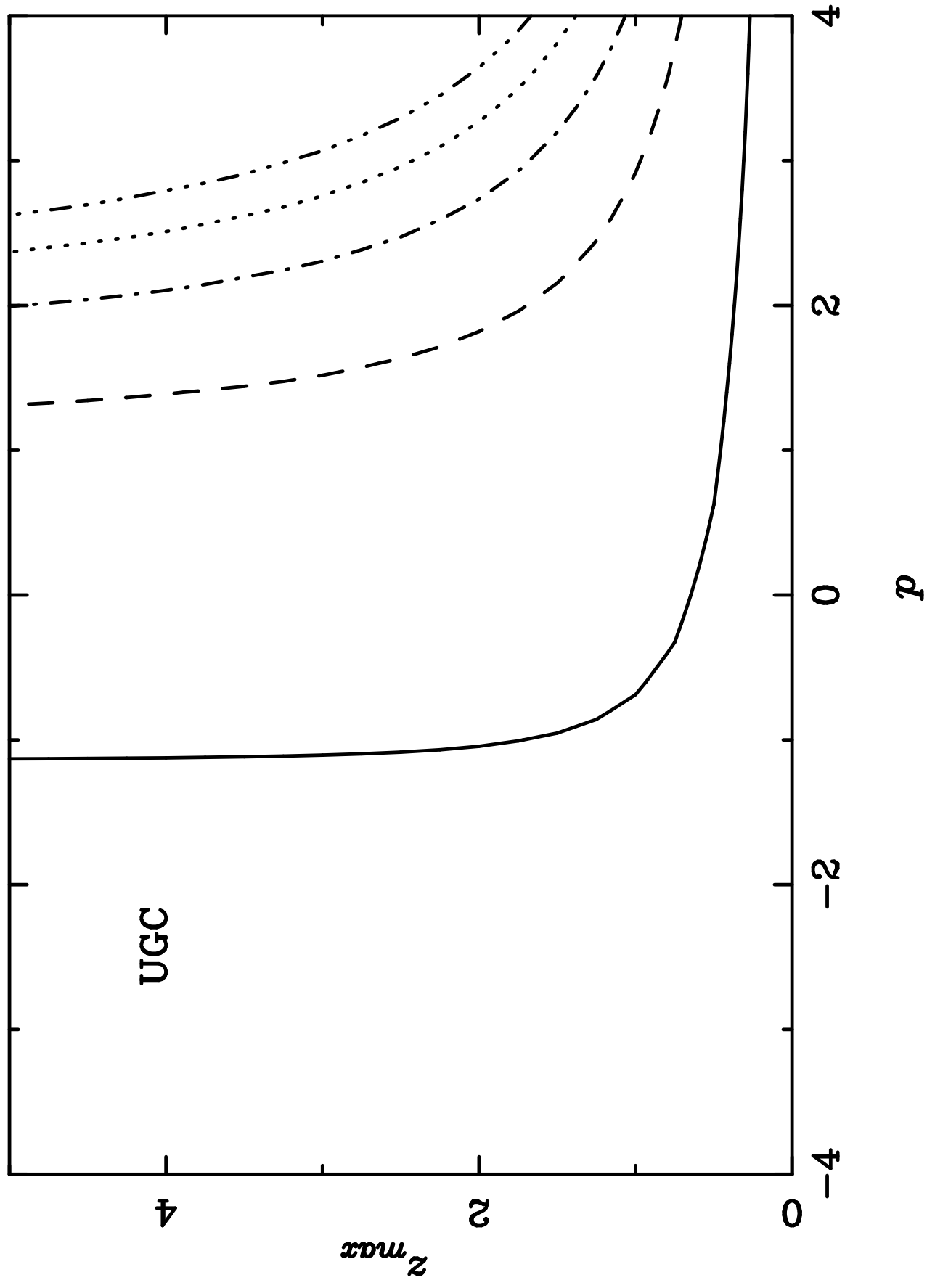


Figure 3b

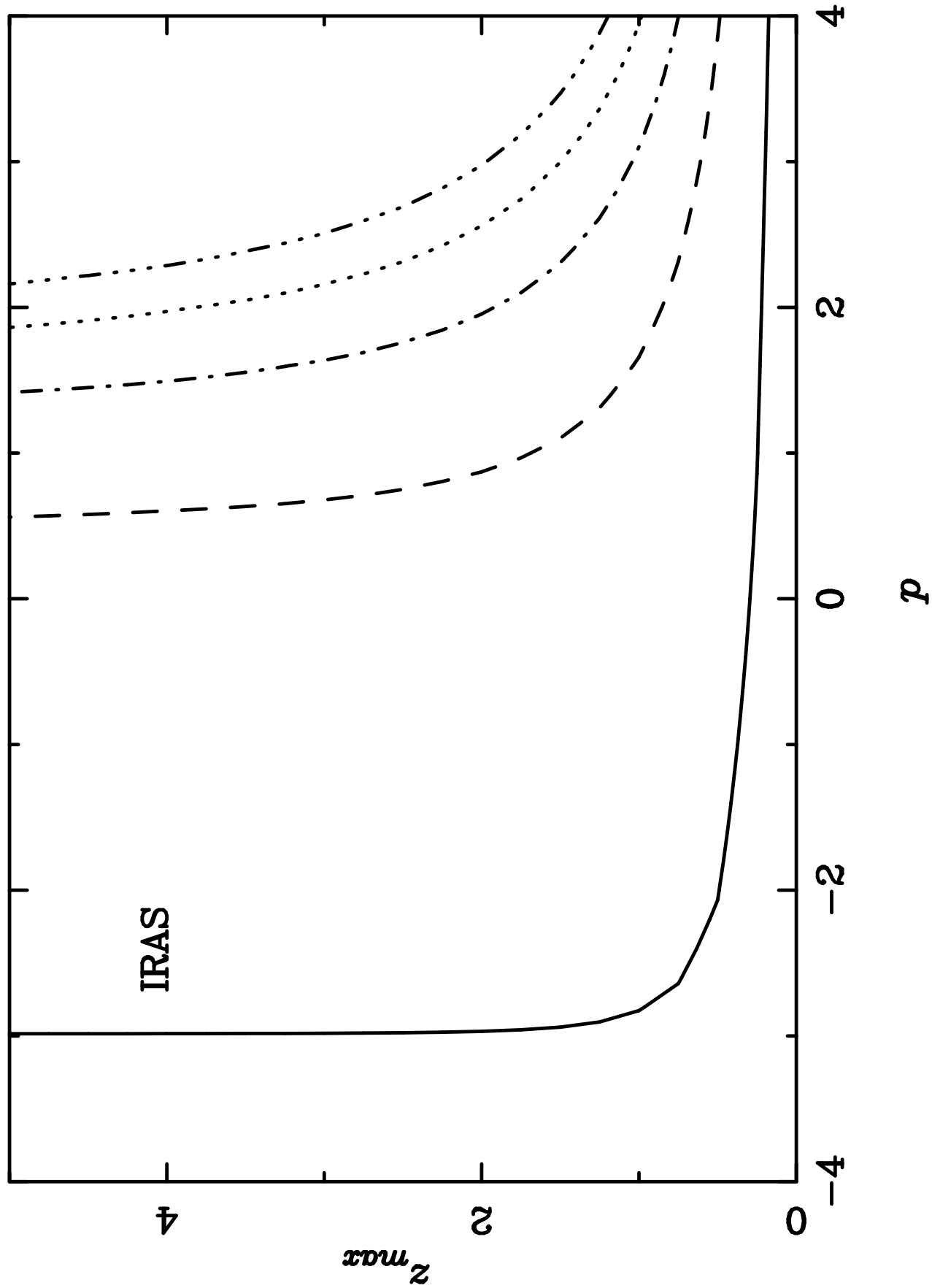


Figure 4

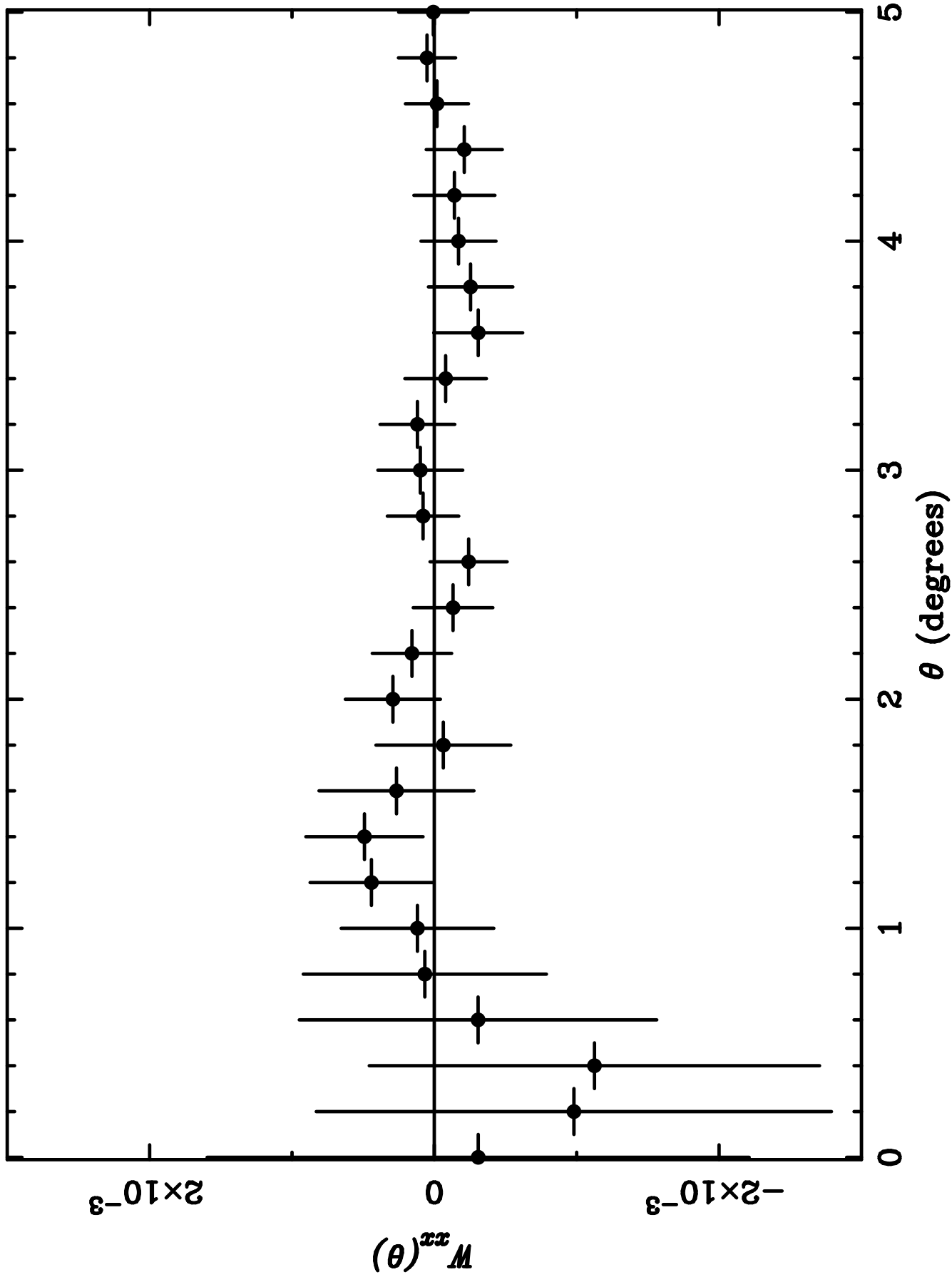


Figure 5a

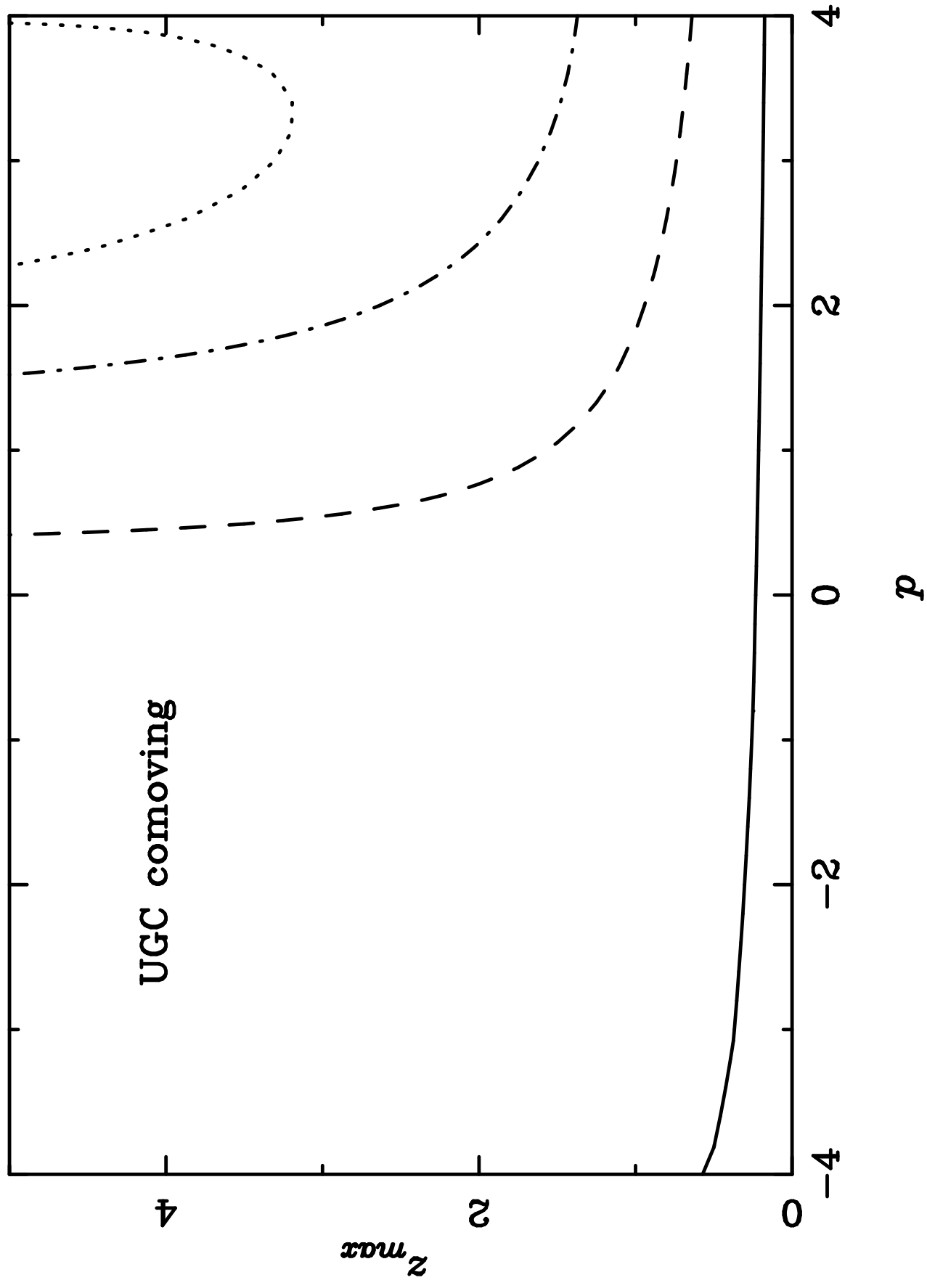


Figure 5b

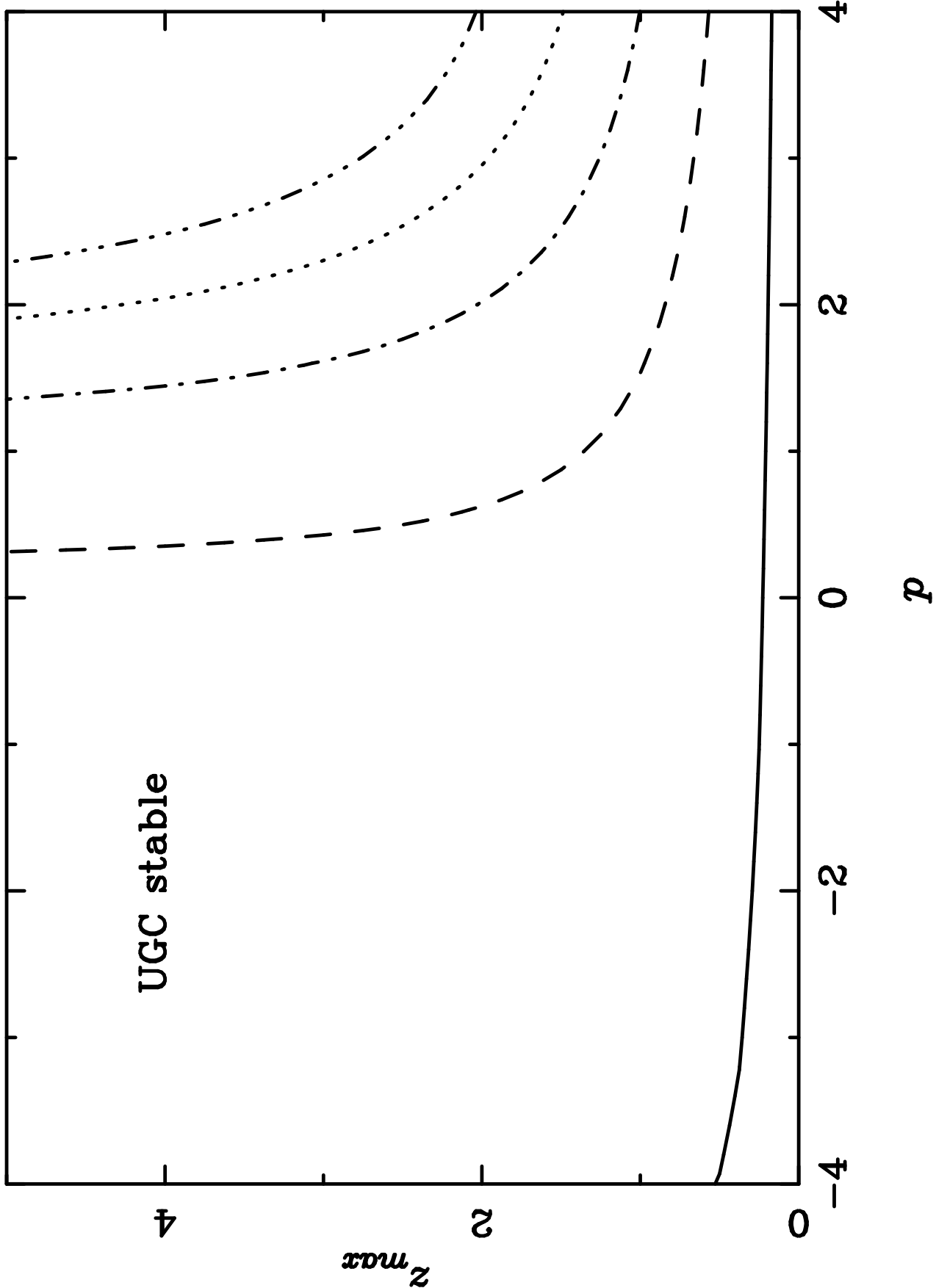


Figure 5c

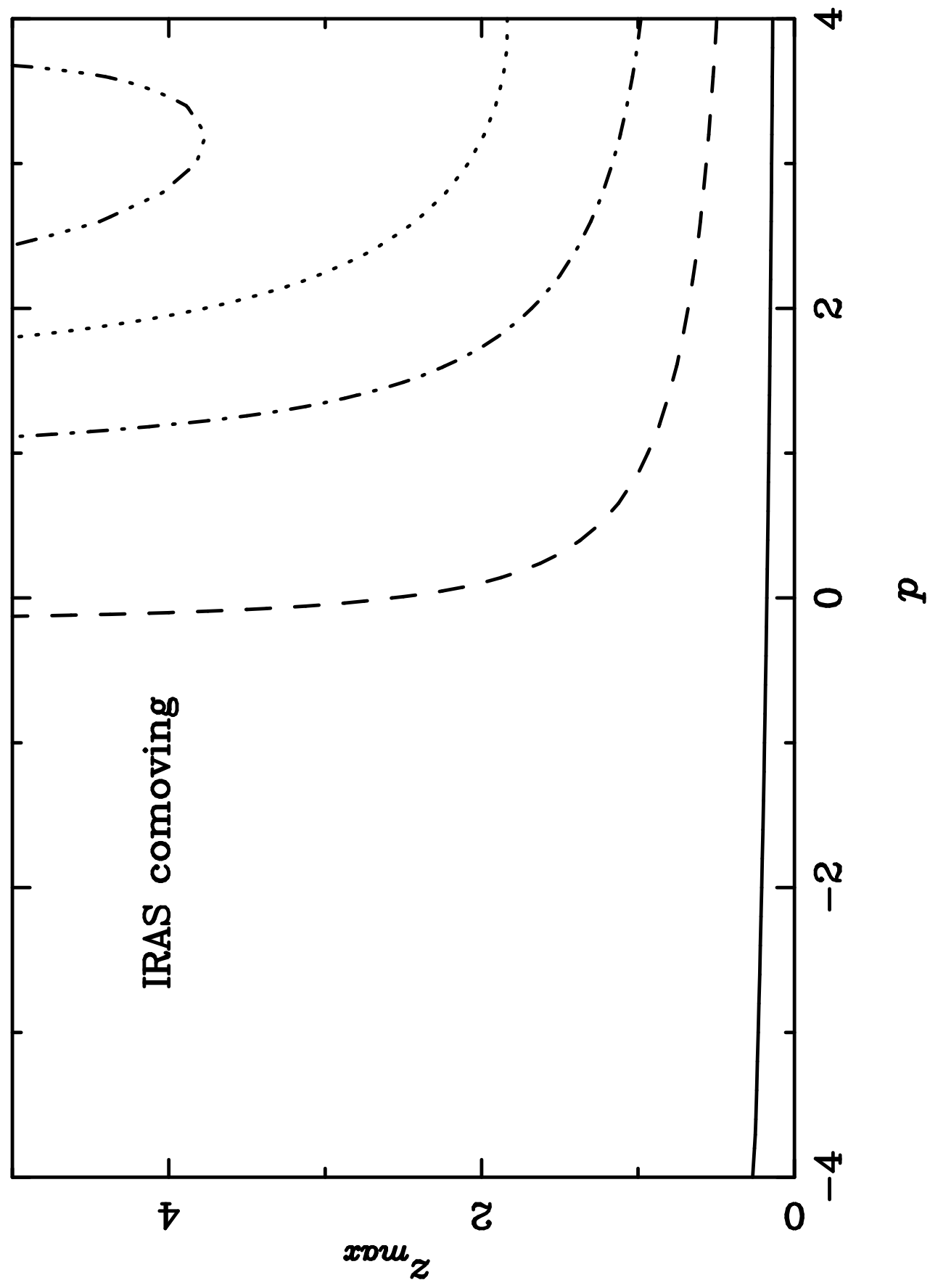


Figure 5d

